

doi: 10.12029/gc20220911001

唐攀, 唐菊兴, 林彬, 李发桥, 孙渺, 祁婧, 崔浩, 王梦蝶, 熊妍, 傅渊慧, 张忠坤, 杨征坤, 姚晓峰, 谢金玲, 陶刚, 杨欢欢. 2024. 西藏甲玛铜多金属矿电气石矿物学特征及其对热液流体演化的指示[J]. 中国地质, 51(4): 1123–1138.

Tang Pan, Tang Juxing, Lin Bin, Li Faqiao, Sun Miao, Qi Jing, Cui Hao, Wang Mengdie, Xiong Yan, Fu Yuanhui, Zhang Zhongkun, Yang Zhengkun, Yao Xiaofeng, Xie Jinling, Tao Gang, Yang Huanhuan. 2024. Mineralogical characteristics of tourmaline in the Jiama copper polymetallic deposit, Tibet: Insights into hydrothermal evolution[J]. Geology in China, 51(4): 1123–1138(in Chinese with English abstract).

西藏甲玛铜多金属矿电气石矿物学特征及其对热液流体演化的指示

唐攀¹, 唐菊兴², 林彬², 李发桥², 孙渺³, 祁婧³, 崔浩⁴, 王梦蝶⁴, 熊妍⁴,
傅渊慧⁵, 张忠坤⁵, 杨征坤⁵, 姚晓峰⁶, 谢金玲⁷, 陶刚¹, 杨欢欢²

(1. 西南科技大学环境与资源学院, 固体废物处理与资源化教育部重点实验室, 四川 绵阳 621010; 2. 中国地质科学院矿产资源研究所, 自然资源部成矿作用与资源评价重点实验室, 北京 100037; 3. 中国地质大学(北京), 北京 100083; 4. 成都理工大学, 四川 成都 610059; 5. 西藏华泰龙矿业开发有限公司, 西藏 拉萨 850212; 6. 中国地质调查局发展研究中心, 北京 100037; 7. 西藏大学, 西藏 拉萨 850000)

提要:【研究目的】角岩作为甲玛超大型斑岩铜多金属成矿系统的重要组成部分, 既是成矿热液的岩性圈闭, 也是重要的赋矿围岩, 但角岩中的电气石成因不明, 对于进一步理解成矿过程有一定制约。【研究方法】本文通过详细的钻孔编录、镜下鉴定和电子探针分析, 研究电气石的成因, 并探讨其对岩浆热液流体演化过程的启示。【研究结果】电气石在甲玛角岩中较为发育, 依据其产状可分为 4 类: Tur-I, 热液角砾岩胶结物中的电气石; Tur-II, 石英+电气石±黄铁矿脉; Tur-III, 电气石±黄铁矿±黄铜矿脉; Tur-IV, 团斑状电气石±黄铁矿; 其中前 3 类电气石较发育环带结构。不同产状电气石均具有较为宽泛的 Al_2O_3 、 $Fe/(Fe+Mg)$ 和 $Na/(Na+Ca)$ 比值, 属于碱基亚类镁电气石和黑电气石, 替代机制为 $x\square Al(NaMg)_{-1}$ 、 $Fe^{2+}Mg_{-1}$ 和 $Fe^{3+}Al_{-1}$ 。【结论】不同产状电气石发育复杂的环带结构, 且成分变化极大, 表明其是岩浆热液流体和地层流体不同程度混合造成的, 且岩浆热液流体与还原性的角岩地层发生的水岩反应可能在甲玛成矿过程中起了重要作用。甲玛不同产状电气石的结构和成分信息记录了岩浆热液演化过程的细节信息, 为完善成矿过程提供了重要证据。

关键词: 电气石; 岩浆热液演化; 斑岩成矿系统; 甲玛铜多金属矿; 冈底斯成矿带; 矿产勘查工程; 西藏

创新点: 不同产状电气石的结构和成分信息示踪斑岩成矿系统热液演化过程。

中图分类号: P618.2 文献标志码: A 文章编号: 1000–3657(2024)04–1123–16

Mineralogical characteristics of tourmaline in the Jiama copper polymetallic deposit, Tibet: Insights into hydrothermal evolution

收稿日期: 2022–09–11; 改回日期: 2022–10–28

基金项目: 国家重点研发计划项目(2022YFC2905004)、四川省自然科学基金(23NSFSC4281)、西南科技大学科研基金(22zx7127)、国家自然科学基金科研项目(41902097、42072313、41902101)、中国地质科学院矿产资源研究所基本科研业务费(KJ2102、KK2017)及大宗紧缺战略性矿产重点调查区块优选(重要矿山深部预测及外围勘查区块优选)(DD20230362)联合资助。

作者简介: 唐攀, 男, 1989 年生, 副教授, 主要从事斑岩-矽卡岩矿床勘查和综合研究; E-mail: tangpan168@163.com。

通讯作者: 唐菊兴, 男, 1964 年生, 研究员, 主要从事矿产勘查和综合研究; E-mail: tangjuxing@126.com。

TANG Pan¹, TANG Juxing², LIN Bin², LI Faqiao², SUN Miao³, QI Jing³, CUI Hao⁴,
WANG Mengdie⁴, XIONG Yan⁴, FU Yuanhui⁵, ZHANG Zhongkun⁵, YANG Zhengkun⁵,
YAO Xiaofeng⁶, XIE Jinling⁷, TAO Gang¹, YANG Huanhuan²

(1. The Key Laboratory of the Ministry of Education on Solid Waste Treatment and Recycling, School of Environment and Resource, Southwest University of Science and Technology, Mianyang 621010, Sichuan, China; 2. MNR Key Laboratory of Metallogeny and Mineral Assessment, Institute of Mineral Resources, Chinese Academy of Geological Sciences, Beijing 100037, China; 3. China University of Geosciences, Beijing 100083, China; 4. Chengdu University of Technology, Chengdu 610059, Sichuan, China; 5. Tibet Huatailong Mining Corp. Ltd., Lhasa 850212, Tibet, China; 6. Development and Research Centre, China Geological Survey, Beijing 100037, China; 7. Tibet University, Lhasa 850000, Tibet, China)

Abstract: This paper is the result of mineral exploration engineering.

[Objective] Hornfels, as an important part of the Jima porphyry copper polymetallic system, is host rocks and a lithologic trap for ore-forming fluid. However, the origin of tourmaline in hornfels is unknown, which restricts the further understanding of the mineralization. **[Methods]** We carried out detailed drilling logging, petrographic observations and major element analyses of tourmaline with distinctive occurrences in hornfels from the Jiama deposit to elucidate the genesis of tourmaline and evolution of magmatic hydrothermal fluids. **[Results]** Four types of tourmalines in hornfels from the Jiama deposit have been identified in this study: 1) Tur-I, tourmaline occurring as cement in hydrothermal breccias; 2) Tur-II, quartz + tourmaline ± pyrite vein; 3) Tur-III, tourmaline ± pyrite ± chalcopyrite vein; 4) porphyritic tourmaline ± pyrite. Tourmaline with distinctive occurrences in hornfels, which belongs to alkali group and dravite-schorl solid solution series, has a wide range of Al₂O₃, Fe/(Fe+Mg) and Na/(Na+Ca). $X_{\square}Al(NaMg)_{-1}$, Fe²⁺Mg₋₁ and Fe³⁺Al₋₁ exchange dominates the substitutions of Tur-I-IV. **[Conclusions]** Tourmaline in hornfels with complicated zoning texture has a very variable compositions, indicating that the tourmaline is caused by different degrees of mixing of magmatic hydrothermal fluid and formation fluid, and the water-rock interaction between magmatic hydrothermal fluid and reduced hornfels may play an important role on the mineralization. The various textures and compositions of tourmaline with distinctive occurrences in hornfels from Jiama record some detailed information related to evolution of magmatic hydrothermal fluid, and can provides evidence for understanding the mineralization.

Key words: tourmaline; evolution of magmatic hydrothermal fluid; porphyry metallogenic system; Jiama copper polymetallic deposit; Gangdese metallogenic belt; mineral exploration engineering; Tibet

Highlights: The various textures and compositions of tourmaline trace evolution of magmatic hydrothermal fluid.

About the first author: TANG Pan, male, born in 1989, associate professor, mainly engaged in research of exploration and evaluation of porphyry-skarn deposit; E-mail: tangpan168@163.com.

About the corresponding author: TANG Juxing, male, born in 1964, professor, mainly engaged in study of mineral deposit and exploration; E-mail: tangjuxing@126.com.

Fund support: Supported by National Key Research and Development Program of China (No.2022YFC2905004), the Natural Science Foundation of Sichuan (No.23NSFSC4281), Research Fund of Southwest University of Science and Technology (No.22zx7127), the National Natural Science Foundation of China (No.41902097, No.42072313, No.41902101), the Basic Research Service Fee of the Chinese Academy of Geological Sciences (No.KJ2102, No.KK2017), and Selection of Key Survey Blocks for Strategic Minerals in Short Supply (Prediction of Deep Part of Important Mines and Selection of Peripheral Exploration Blocks) (No. DD20230362).

1 引 言

电气石是一种分子结构和化学成分复杂的硼硅酸盐矿物,既可以形成于岩浆阶段,也可以形成

于热液蚀变过程(Launay et al., 2018; Han et al., 2020; 李真真等, 2020; Qiu et al., 2021),其化学通式为 XY₃Z₆[T₆O₁₈][BO₃]₃V₃W, 其中 X=Na⁺, Ca²⁺, K⁺, □[空位]; Y=Fe²⁺, Mg²⁺, Mn²⁺, Al³⁺, Li⁺, Fe³⁺, Ti⁴⁺;

$Z=Al^{3+}, Fe^{3+}, Mg^{2+}; T=Si^{4+}, Al^{3+}, (B^{3+}); V=OH^{-}, O^{2-}; W=OH^{-}, O^{2-}, F^{-}$ (Henry et al., 2011)。电气石是一种物理化学性质稳定的矿物,其结晶后能在极宽的压力-温度(P-T)范围内稳定存在,也能与大多数地质流体平衡(Novák et al., 2011; Dutrow and Henry, 2011; Hinsberg et al., 2011),常分布于火成岩、沉积岩、变质岩和热液矿床中,如花岗岩岩浆热液型 Sn-W 矿床、沉积岩容矿的沉积喷流(SEDEX)型 Pb-Zn-Ag 矿床、与火山岩相关的块状硫化物(VMS)型 Cu-Zb-Pb-Ag-Au 矿床、斑岩型 Cu±Mo±Au 矿床、矽卡岩型 Fe 矿床、硼矿床、伟晶岩型稀有金属矿床、角砾岩筒 Cu±Au 矿床和铁氧铜金(IOCG)矿床等(Griffin et al., 1996; 薛建玲等, 2006; Slack and Trumbull, 2011; Baksheev et al., 2012; Gupta et al., 2014; 于森等, 2016; Yu et al., 2017; 郭佳等, 2020; Zhang et al., 2021; 凤永刚等, 2022)。热液电气石的主微量成分受围岩、外部流体及其结晶时的温度-压力控制(Henry and Guidotti, 1985; Codeço et al., 2017)。因电气石具有宽泛的温度-压力(P-T)形成条件、元素扩散速率低、抗风化性、复杂的化学成分和硼同位素组成,常被用于示踪成矿过程和流体来源(Slack and Trumbull, 2011; Dutrow and Henry, 2011; Codeço et al., 2017; Harlaux et al., 2020)。

青藏高原被誉为“世界的屋脊”,是研究特提斯演化及印度板块和欧亚板块相互作用过程的“天然实验室”(Hou et al., 2003; Zhu et al., 2013)。作为青藏高原最重要的成矿带之一,冈底斯铜多金属成矿带位于拉萨地体南部(图 1a),已成为我国重要的国家级资源基地(Hou et al., 2003; 唐菊兴等, 2017),该带上分布众多新生代的大型—超大型大陆碰撞型斑岩铜钼矿床,如驱龙、甲玛、邦铺等(唐菊兴等, 2010, 2011; Zheng et al., 2016; Yang and Cooke, 2019; Tang et al., 2019, 2021)。甲玛超大型矿床作为冈底斯成矿带的典型代表之一,其斑岩型矿体+角岩型矿体+矽卡岩型矿体金属量:铜大于 1000 万 t,钼 106 万 t,铅+锌 175 万 t,金大于 305 t,伴生银大于 15800 t。甲玛矿床的勘查和综合研究程度较高,前人重点对斑岩型矿体和矽卡岩型矿体开展了大量的研究工作,查明了其成矿机制,构建了相对应的成岩成矿模式(应立娟等, 2010, 2011; 姚

晓峰等, 2014; 郭文铂等, 2014; Zheng et al., 2016; 唐攀等, 2016, 2017; 王艺云等, 2017; 张泽斌等, 2019; 林彬等, 2019, 2021; 张忠坤等, 2021)。作为甲玛斑岩成矿系统重要组成之一的巨厚角岩型矿体铜金属量超过 300 万 t(约占总资源量的 1/3),是国内外少见的规模巨大的产于角岩中的铜钼矿体,也是目前矿山露天开采的主要对象之一。甲玛角岩中发育大量的电气石,且电气石是反演岩浆热液流体演化的指示矿物。此文拟通过研究不同产状电气石矿物显微结构和化学成分组成,初步厘定电气石的成因,并探讨其对岩浆热液流体演化过程的启示。

2 区域地质概况

西藏冈底斯成矿带位于拉萨地体南部(图 1a),指产于冈底斯岩浆弧中的铜金铁钼钨锑铅锌硼成矿带,矿床主要集中在谢通门至工布江达之间,与冈底斯岩浆弧范围相当(唐菊兴等, 2012)。拉萨地体位于雅鲁藏布江缝合带和班公湖—怒江缝合带之间(图 1a),由前寒武纪结晶基底、古生代到中生代海相沉积岩和古生代到新生代岩浆岩组成(Zhang et al., 2014)。三叠纪晚期拉萨地体从冈瓦纳大陆分离,随后经历侏罗纪岛弧造山运动、白垩纪大陆边缘弧叠加、古新世碰撞造山运动、中新世地壳变形,这些构造事件形成了 1500 km 的东西走向的冈底斯构造岩浆带(Zhao et al., 2015)。

冈底斯构造岩浆带是新特提斯洋壳北向俯冲到亚洲大陆之下,以及印度—亚洲大陆碰撞的结果(Yin and Harrison, 2000),主要由晚古新世—早始新世(60~40 Ma)的林布宗组火山岩和白垩纪—古近纪—新近纪的花岗岩基组成(Allegre et al., 1984; Mo et al., 2008)。印度—亚洲碰撞发生多期成矿事件,即形成主碰撞造山成矿作用(65~41 Ma)、晚碰撞转换成矿作用(40~26 Ma)以及后碰撞地壳伸展成矿作用(25~0 Ma)(Chung et al., 2005; 侯增谦等, 2006)。冈底斯成矿带内重要矿床类型,由老到新,主要包括:1)与洋壳俯冲花岗质岩类有关的 Cu-Au 矿床,如雄村(Lang et al., 2014; Xie et al., 2018);2)与俯冲—碰撞弧花岗岩有关的 Cu-Fe-Pb-Zn 矿床,如新嘎果、日阿、拉屋、亚贵拉等(Wang et al., 2018; Tang et al., 2020);3)与碰撞造山后期伸展背景花岗质斑岩有关 Cu-Mo-Au 矿床,

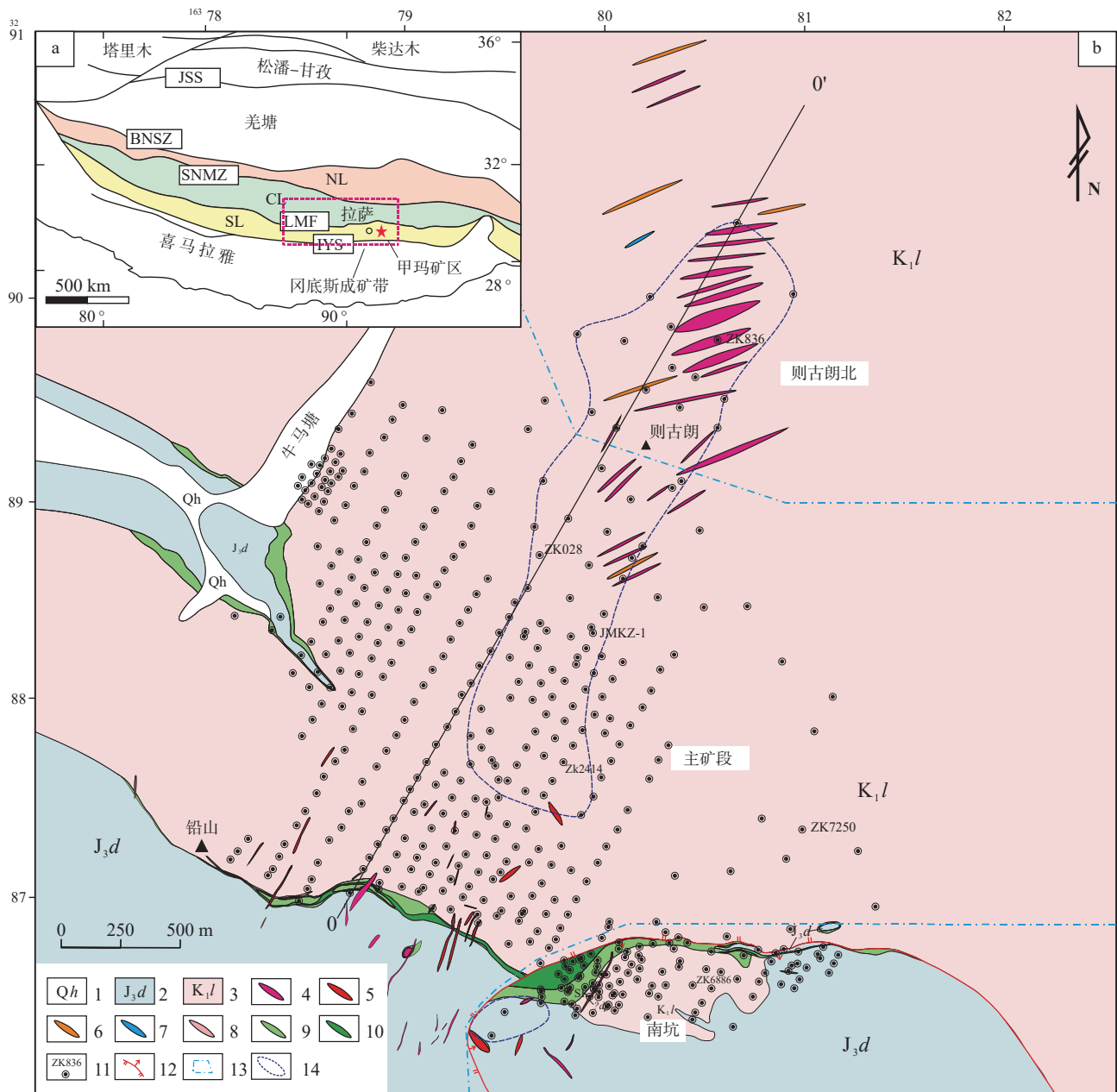


图1 甲玛矿区大地构造位置简图(a)及地质图(b)(据唐菊兴等, 2010 修改)

1—第四系残坡积物; 2—多底沟组大理岩、灰岩; 3—林布宗组板岩、角岩; 4—花岗闪长斑岩; 5—花岗斑岩; 6—石英闪长玢岩; 7—煌斑岩; 8—细晶岩; 9—矽卡岩; 10—矽卡岩矿体; 11—钻孔及编号; 12—滑覆构造; 13—矿段; 14—隐伏岩体范围; JSS—金沙江缝合带; BNSZ—班公湖—怒江缝合带; SNMZ—狮泉河—嘉黎蛇绿岩混杂岩带; LMF—洛巴堆—米拉山断裂带; IYS—印度—雅鲁藏布江缝合带; SL—南拉萨地体; CL—中拉萨地体; NL—北拉萨地体

Fig.1 Tectonic location (a) and geological map (b) of Jiama ore district (modified from Tang Juxing et al., 2010)

1—Quaternary; 2—Marble and limestone of Duodigou Formation; 3—Slate and hornfels of Linbuzong Formation; 4—Granodiorite porphyry; 5—Granite porphyry; 6—Quartz diorite porphyry; 7—Lamprophyre; 8—Aplite; 9—Skarn; 10—Skarn ore-body; 11—Drilling and number; 12—Slip fault; 13—Segment of mining; 14—Concealed intrusive outline; JSS—Jinsha suture zone; BNSZ—Bangong—Nujiang suture zone; SNMZ—Shiquan River—Nam Tso mélange zone; LMF—Luobadui—Milashan Fault; IYS—Indus—Yarlung Zangbo suture zone; SL—Southern Lhasa subterrane; CL—Central Lhasa subterrane; NL—Northern Lhasa subterrane

如厅宫、冲江、甲玛、驱龙、邦铺等 (Yang et al., 2009; Zheng et al., 2016; Tang et al., 2019, 2021)。

其中, 与碰撞造山后期伸展背景下形成的斑岩型矿床是冈底斯成矿带的突出代表 (唐菊兴等, 2017)。

3 矿床地质

3.1 地层

甲玛矿区出露地层较简单, 主要为一套碎屑—碳酸盐岩沉积岩系: 上侏罗统多底沟组(J_3d)灰岩、大理岩, 主要分布于矿区南侧; 下白垩统林布宗组(K_1l)砂板岩、板岩、角岩, 分布于矿区中部和北部; 第四系(Q), 主要分布于牛马塘一带(图 1)。

3.2 构造

构造对甲玛铜多金属矿的形成至关重要。甲玛矿床受控于甲玛—卡军果逆冲推覆构造和铜山滑覆构造。其中, 甲玛—卡军果推覆构造主要指矿区由北向南形成一系列逆冲推覆褶皱构造, 其强变形的年龄大致为 50 Ma(钟康惠等, 2012), 与印度板块—欧亚板块碰撞有关(Yin and Harrison, 2000; Mo et al., 2007)。推覆构造形成的牛马塘倒转背斜和层间构造, 分别控制斑岩体的侵位以及 I 号矽卡岩主矿体的空间产出形态。铜山滑覆构造是由于逆冲推覆过程中, 铜山块体重力失稳向北滑覆形成, 滑覆体内部形成大量的次级褶皱、裂隙(钟康惠等, 2012), 主要控制着南坑矿段的 II 号矽卡岩矿体空间产出形态(Zheng et al., 2016)。

3.3 岩浆岩

矿区岩浆岩主要为中新世的中酸性复式斑岩体, 岩性主要为花岗闪长斑岩、二长花岗斑岩和石英闪长玢岩, 以及少量的闪长岩、辉绿玢岩、煌斑岩和细晶岩等, 整体呈近南北向分布。大部分岩体隐伏产出, 与铜山—马拉日一带的角岩密切相关。与矿化有关的岩体为花岗闪长斑岩、二长花岗斑岩和石英闪长玢岩, 其中二长花岗斑岩与钼矿化有关, 花岗闪长斑岩和石英闪长玢岩与铜矿化关系密切。

3.4 蚀变

甲玛矿区的热液蚀变主要为钾化、绢英岩化、绢云母—绿泥石化、青磐岩化、电气石化、泥化(图 2)。钾化主要产于花岗闪长斑岩、二长花岗斑岩、石英闪长玢岩及角岩中, 蚀变矿物组合主要为黑云母、石英, 少量的钾长石、石膏、磁铁矿、黄铜矿、辉钼矿、黄铁矿。绢英岩化主要产于斑岩和角岩中, 位于钾化蚀变之上, 并且部分叠加于钾化之

上, 蚀变矿物组合主要为绢云母、石英, 少量的黄铁矿、黄铜矿、辉钼矿。绢云母—绿泥石化主要产于浅部角岩中, 位于钾化和绢英岩化的外围, 蚀变矿物组合主要为绿泥石、绢云母, 少量的磁铁矿、黄铜矿、黄铁矿、方解石。电气石化规模较小, 主要发育于角岩中, 矿物组合主要为电气石, 少量的方解石, 黄铜矿、黄铁矿。青磐岩化主要产于浅部斑岩中, 蚀变矿物组合为绿泥石、绿帘石, 少量的方解石和黄铁矿。泥化规模较小, 主要发育于古朗浅地表, 部分沿着裂隙分布于角岩和斑岩中, 蚀变矿物主要为高岭石, 少量的绢云母。

3.5 矿体

甲玛斑岩成矿系统矿体包括矽卡岩型铜多金属矿体、角岩型铜钼矿体、斑岩型钼(铜)矿体、外围独立金矿体以及规模较小的 Manto 型矿体(图 2)。矽卡岩型矿体根据不同的控矿构造, 进一步分为 I 号矽卡岩矿体和 II 号矽卡岩矿体。I 号矽卡岩矿体是最主要的矿体, 形成于斑岩体和多底沟组大理岩的接触带以及林布宗组角岩和多底沟组大理岩的层间滑脱带; 矿体呈层状、似层状、厚板状, 总体走向为北西—南东, 延长约 3000 m, 矿体倾向北东, 延伸大于 2000 m。II 号矽卡岩矿体产于铜山滑覆体内, 是近年继揭露深部斑岩矿体之后的又一找矿重大突破; 矿体走向西—南东, 延长约 700 m, 倾向北北东, 延伸大于 700 m; 矿体形态不规则, 并且变化较大, 整体呈巨厚的透镜体。斑岩矿体包含两个矿体, IV 和 VI 号矿体, 分别受 1[#]和 2[#]号斑岩体控制, 呈筒状产于矿区中部, 垂向延伸大于 600 m。角岩矿体围绕斑岩体分布, 包括 3 个矿体, 分别为 III 号矿体、V-1 号矿体和 V-2 号矿体, 呈筒状。

3.6 电气石类型

甲玛矿区角岩中产出大量的电气石, 根据产出特征, 可分为 4 类。(1)Tur-I: 热液角砾岩胶结物中电气石, 黑色, 且具放射状外形; 在镜下, 呈半自形—自形, 粒径大小 0.2~0.5 mm, 具有黄棕到黄绿色多色性, 无明显环带(图 3a-b, 图 4a)。(2)Tur-II: 石英+电气石±黄铁矿脉, 黑色, 且具放射状、长条状或不规则状外形; 在镜下, 呈半自形—自形与石英、黄铁矿共生, 粒径大小 0.02~1 mm, 具有黄棕到黄绿色多色性, 具有明显环带(图 3c-f, 图 4b)。(3)Tur-III:

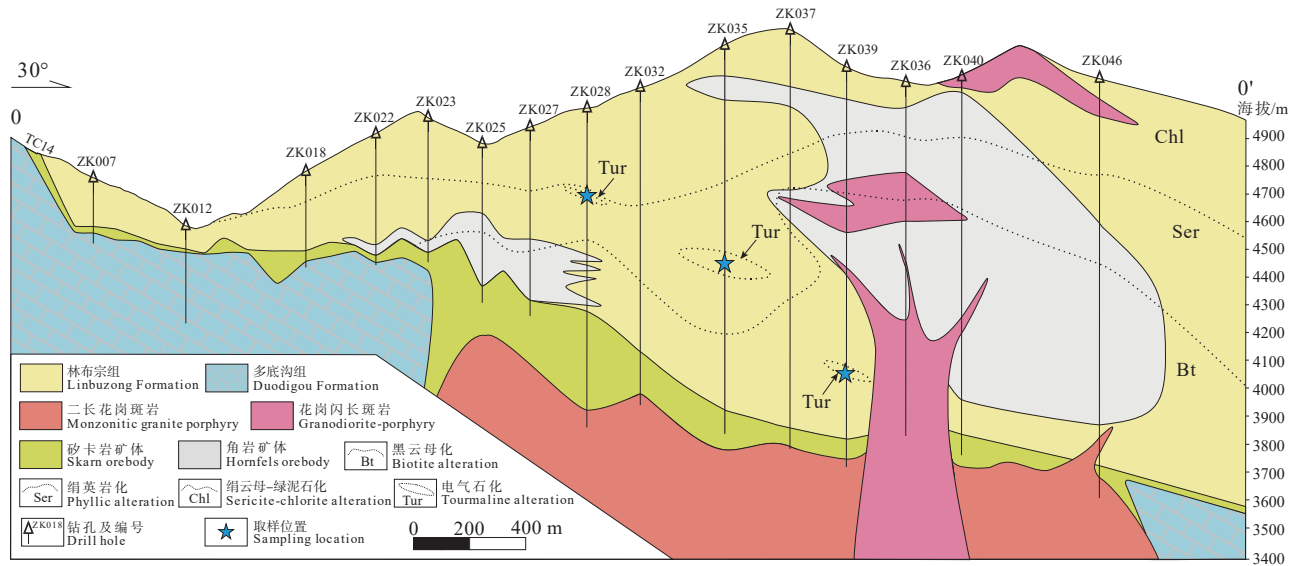


图 2 甲玛矿区 0 号勘探线地质剖面图

Fig.2 Geological cross section along No.0 prospecting line of Jiama ore district

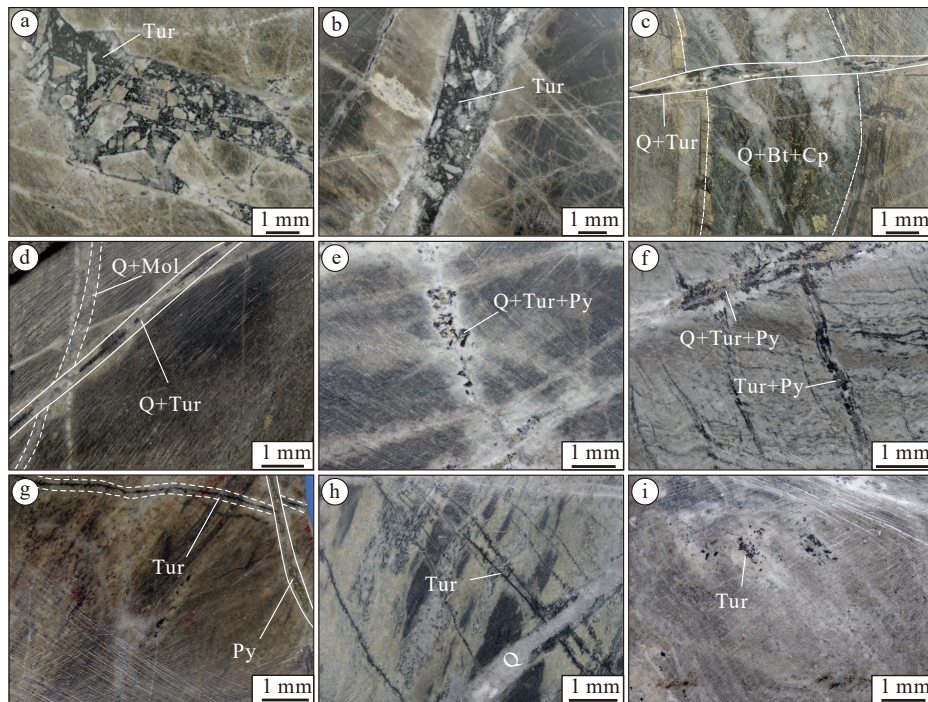


图 3 甲玛矿区不同产状电气石标本照片

a~b—热液角砾岩胶结物中电气石(Tur-I); c—石英+电气石脉(Tur-II), 切穿早期的石英+黑云母+黄铜矿脉; d—石英+电气石脉(Tur-II), 切穿早期的石英+辉钼矿脉; e—石英+电气石+黄铁矿脉(Tur-II); f—石英+电气石+黄铁矿脉(Tur-II)和电气石+黄铁矿脉(Tur-III); g—电气石脉(Tur-III), 被后期的黄铁矿脉切穿; h—电气石脉(Tur-III), 被后期的无矿石英脉切穿; i—团斑状电气石+黄铁矿(Tur-IV); Tur—电气石; Py—黄铁矿; Cp—黄铜矿; Q—石英; Bt—黑云母; Mol—辉钼矿

Fig.3 Hand specimens of tourmalines with different occurrences of Jiama deposit

a~b—Tourmaline occurring as cement in hydrothermal breccias (Tur-I); c—Quartz + tourmaline vein (Tur-II) cutting quartz + biotite + chalcopyrite vein; d—Quartz + tourmaline vein (Tur-II) cutting quartz + molybdenite vein; e—Quartz + tourmaline + pyrite vein (Tur-II); f—Quartz + tourmaline + pyrite vein (Tur-II) and tourmaline + pyrite vein (Tur-III); g—Tourmaline vein (Tur-III) cut by pyrite vein; h—Tourmaline vein (Tur-III) cut by quartz vein; i—Porphyritic tourmaline + pyrite (Tur-IV); Tur—Tourmaline; Py—Pyrite; Cp—Chalcopyrite; Q—Quartz; Bt—Biotite; Mol—Molybdenite

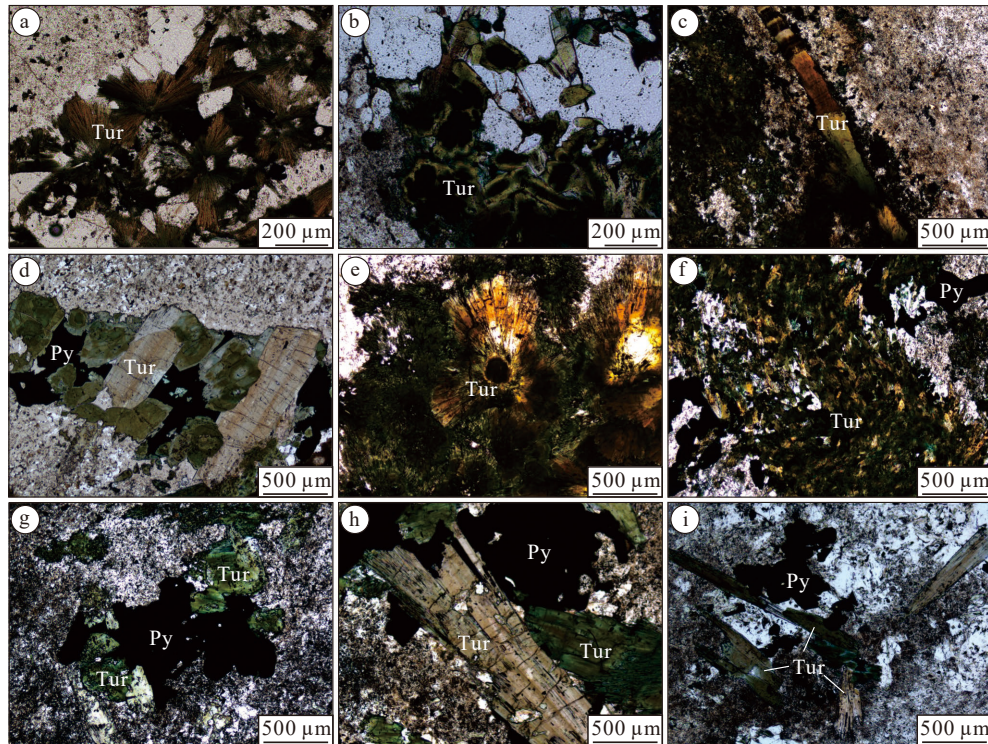


图 4 甲玛矿区不同产状电气石镜下照片

a—热液隐爆角砾岩胶结物中放射状电气石; b—石英+电气石脉, 电气石半自形—自形, 具有环带结构; c—电气石脉; d—电气石+黄铁矿脉, 电气石半自形—自形, 具有环带结构; e—电气石脉, 电气石呈放射状; f—电气石+黄铁矿脉, 电气石呈他形—半自形; g—团斑状电气石+黄铁矿, 电气石呈他形; h—i—团斑状电气石+黄铁矿, 电气石呈半自形—自形

Fig.4 Microphotos of tourmalines with different occurrences of Jiama deposit

a—Tur-I with radial texture; b—Euhedral to subhedral Tur-II shows distinct zoning texture; c—Fine-grained Tur-III; d—Euhedral to subhedral Tur-III shows distinct zoning texture and coexist with pyrite; e—Tur-III with radial texture; f—Fine-grained, subhedral and anhedral Tur-III coexist with pyrite; g—Anhedral Tur-IV coexist with pyrite; h—i—Subhedral and anhedral Tur-IV coexist with pyrite

电气石±黄铁矿±黄铜矿脉, 黑色, 且具长条状或不规则状外形; 在镜下, 呈他形—半自形, 部分与黄铁矿、黄铜矿共生, 粒径大小 0.02~0.1 mm, 具有黄棕到黄绿色多色性, 无明显环带(图 3f~h, 图 4c~f)。(4)Tur-IV: 团斑状电气石±黄铁矿, 黑色, 且具长条状或不规则状外形; 在镜下, 呈半自形—自形与黄铁矿共生, 分布于石英、长石等角岩矿物之间, 粒径大小 0.2~0.6 mm, 具有黄棕色到黄绿色多色性, 无明显环带, 常与黄铁矿共生产出(图 3i, 图 4g~i)。

4 样品及分析方法

本次研究工作通过钻孔岩心编录确定电气石的产出特征, 然后采集不同钻孔深度的角岩中电气石样品。全部样品切片后, 经过系统的镜下鉴定, 结合背散射查明电气石的形貌特征、环带、共生矿物组合。最后, 基于电气石的显微结构特征, 开展

电子探针实验。

电气石主量元素成分分析在中国地质科学院矿产资源研究所电子探针实验室完成, 测试仪器为 JXA-8230 电子探针仪。仪器工作条件: 加速电压 15 kV, 加速电流 20 nA, 束斑直径 5 μm 。测试元素为 Si、Ti、Al、Cr、Fe、Mg、Ca、Mn、Ba、Na、F、Cl。以下天然矿物作为标定矿物: 磷灰石(P、Ca)、石英(Si)、硬玉(Na)、镁铝榴石(Mn)、磁铁矿(Fe)、钛铁矿(Ti)、铬铁矿(Cr)、石盐(Cl)、萤石(F)。

5 分析结果

本文电气石分子式的计算基于理想分子式以 31 个阴离子(O、OH、F)为基础计算, B_2O_3^* 和 H_2O 含量分别基于 $\text{B}=3$ 和 $\text{OH}+\text{F}+\text{Cl}=4$ 计算获得(Henry and Dutrow, 1996), 计算结果见表 1。

甲玛角岩中不同产状电气石的主量成分变化

较大, SiO_2 为 26.34%~37.71% (平均值 34.61%), Al_2O_3 为 18.88%~38.50% (平均值 30.72%), MgO 为 2.05%~10.47% (平均值 6.55%), FeO_T 为 3.06%~21.78% (平均值 10.39%), Na_2O 为 1.86%~2.71% (平均值 2.41%), CaO 为 0.04%~1.44% (平均值 0.62%), TiO_2 为 0.05%~2.89% (平均值 0.74%), 挥发分 F 含量较低 0%~0.22% (平均值 0.06%)。根据电气石 X 位置阳离子的占位情况 (Henry et al., 2011), 甲玛

角岩中不同产状电气石均落在碱基电气石区域范围内 (图 5a)。在 Al-Fe-Mg 三元图解中, 4 种产状的电气石主要落于 2 区和 4 区, 即贫锂的花岗岩/伟晶岩和含 Al 饱和矿物的变泥质岩环境 (图 5b)。在 $\text{Fe}/(\text{Fe}+\text{Mg})-x/(Na+K+x)$ 和 $\text{Fe}/(\text{Fe}+\text{Mg})-\text{Na}/(\text{Na}+\text{Ca})$ 分类图解中, Tur-I 电气石投于黑电气石区域; Tur-II 电气石投于镁电气石和黑电气石区域; Tur-III 电气石主要投于镁电气石和黑电气石区域,

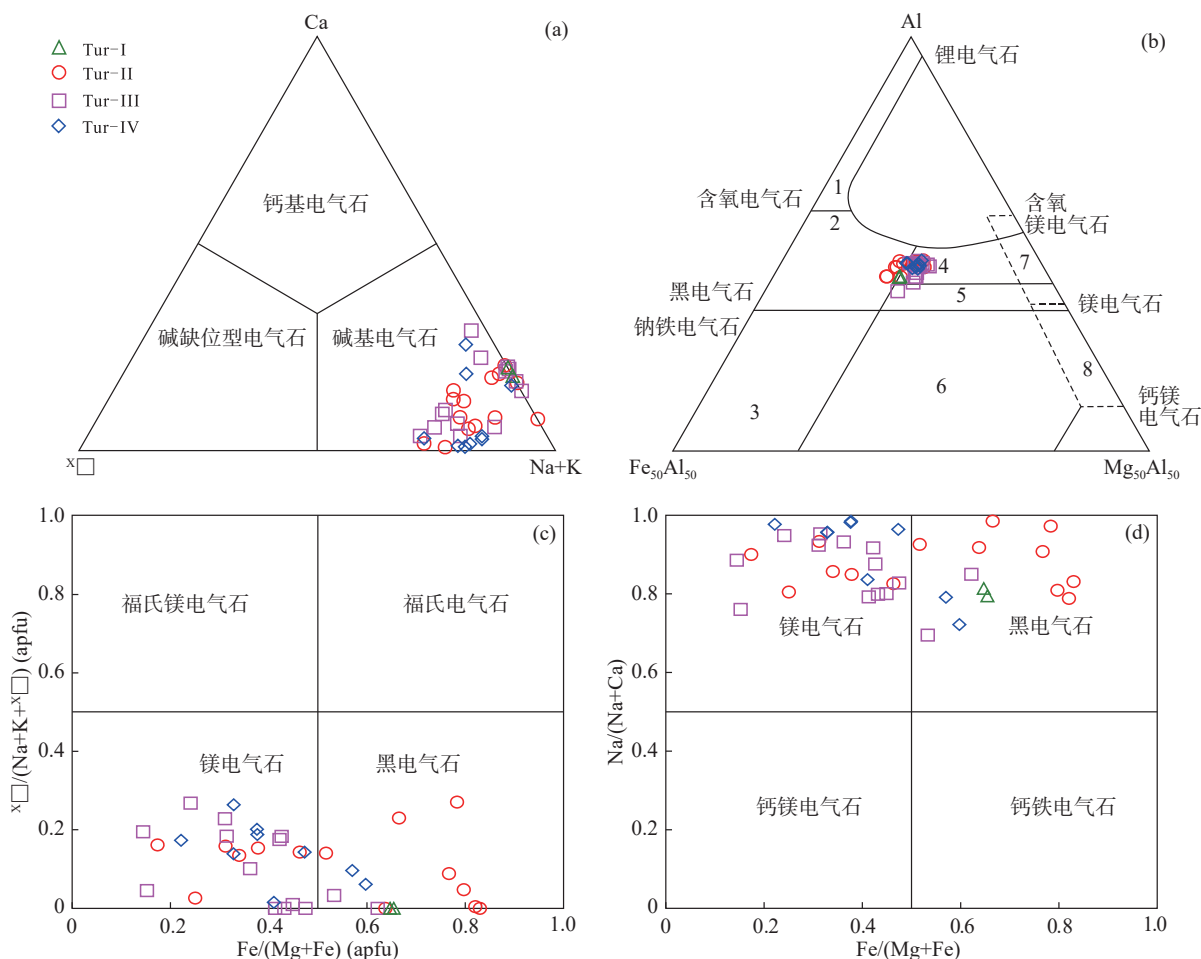


图 5 甲玛矿区不同产状电气石分类图解

a— $\text{Ca}-x-(Na+K)$ 三元图解 (底图据 Henry et al., 2011); b— $\text{Al}-\text{Fe}-\text{Mg}$ 图解 (底图据 Henry and Guidotti, 1985), 图中 1、2 区分别代表富 Li 和贫 Li 花岗岩和伟晶岩、细晶岩, 3 区为富 Fe^{3+} 的石英-电气石岩 (热液蚀变花岗岩), 4、5 区分别代表含 Al 饱和矿物相和不含 Al 饱和矿物相的变泥质岩和变砂屑岩, 6 区代表富 Fe^{3+} 的石英-电气石岩、钙质硅酸岩和变泥质岩, 7 区代表贫 Ca 变质超镁铁岩和富 Cr、V 的变质沉积岩, 8 区代表变质碳酸盐和变质辉石; c— $\text{Fe}/(\text{Fe}+\text{Mg})-x/(Na+K+x)$ 图解 (底图据 Henry et al., 2011); d— $\text{Fe}/(\text{Fe}+\text{Mg})-\text{Na}/(\text{Na}+\text{Ca})$ 图解 (底图据 Henry et al., 2011)

Fig. 5 Tourmaline discrimination diagrams with different occurrences of Jiama deposit

a— $\text{Ca}-x-(Na+K)$ diagram for tourmaline discrimination (after Henry et al., 2011); b—Plot $\text{Al}-\text{Fe}-\text{Mg}$ for tourmaline from various rock types (after Henry and Guidotti, 1985), 1—Li-rich granitoid pegmatites and aplites; 2—Li-poor granitoid rocks and associated pegmatites and aplites; 3— Fe^{3+} -rich quartz-tourmaline rocks (hydrothermally altered granites); 4—Metapelites and metapsammities coexisting with an Al-saturating phase; 5—Metapelites and metapsammities not coexisting with an Al-saturating phase; 6— Fe^{3+} -rich quartz-tourmaline rocks, calcsilicate rocks, and metapelites; 7—Low-Ca metaultramafic rocks and Cr, V-rich metasediments; 8—Metacarbonates and meta-pyroxenites; c— $\text{Fe}/(\text{Fe}+\text{Mg})-x/(Na+K+x)$ diagram for tourmaline discrimination (after Henry et al., 2011); d— $\text{Fe}/(\text{Fe}+\text{Mg})-\text{Na}/(\text{Na}+\text{Ca})$ diagram for tourmaline discrimination (after Henry et al., 2011)

2 个点投于黑电气石区域; Tur-IV 电气石主要投于镁电气石区域, 2 个点投于黑电气石区域(图 5c~d)。四种产状电气石的 Al-Fe 和 Mg-Fe 图解, 显示甲玛电气石为 $\text{Fe}^{2+}\text{Mg}_{-1}$ 和 $\text{Fe}^{3+}\text{Al}_{-1}$ 的替代方式; 而四种产状电气石的 Al-Fe 和 Al-Na 图解, 显示甲玛电气石还存在 $\text{Al}(\text{NaMg})_{-1}$ 的替代方式(图 6)。

6 讨论

6.1 电气石的成因

甲玛矿区角岩是热接触变质作用的产物(原岩为林布宗组板岩), 围绕隐伏岩体产出, 分布范围广, 面积近 5 km^2 , 作为矽卡岩型矿体的顶板, 既是成矿热液的岩性圈闭, 也是重要的赋矿围岩(唐菊兴等, 2011; 王登红等, 2011), 是甲玛斑岩成矿系统的重要组成部分。甲玛角岩中发育大量的电气石, 电气石化主要产于绢英岩化带和钾化带。此外, 由穿插关系可知, 电气石脉切穿了早期的石英+黑云母(A 脉)和石英+辉钼矿脉(B 脉), 但被晚期的黄铁矿脉(D 脉)切穿, 脉状电气石形成于 B 脉和 D 脉之间。因此, 电气石不可能形成于角岩变质阶段, 而是与岩浆热液流体有关, 属于热液成因。

研究表明, 围岩性质是控制岩浆热液成因电气石化学组成的重要因素, 电气石的 Fe、Mg、Mn 等主微量成分在一定程度上能够揭示其赋存母岩的化学组成(van Hinsberg et al., 2011)。尽管岩浆演化晚期熔体中 B 含量可达到百分之几, 但由于酸性岩浆中 Fe-Mg 含量低, 仅靠岩浆出溶流体并不能在

围岩中形成大量电气石, 还需要围岩地层提供大量的 Fe-Mg-Ca 等成分(London and Manning, 1995; Yu and Jiang, 2003; Jia et al., 2010; Codeço et al., 2017)。甲玛斑点状原生黑云母角岩原岩为林布宗组板岩, 其成分具有较高的 SiO_2 (平均值 62.66%)、 Al_2O_3 (平均值 17.65%) 和 FeO_T (平均值 5.89%), 较低的 MgO(平均值 2.15%)、CaO(平均值 2.30%)、 Na_2O (平均值 2.26%)(王崑平和唐菊兴, 2011)。甲玛原生黑云母角岩具有较高的 FeO_T 含量与角岩中的原生变质黑云母具有富铁的特征(唐攀等, 2016)相吻合。甲玛矿区电气石成分主要投于 Al-Fe-Mg 三元图解中贫锂的花岗岩/伟晶岩和含 Al 饱和矿物的变泥质岩环境区域(图 5b), 与电气石的围岩为角岩相吻合, 且与形成电气石的热液流体有关的岩浆也是贫锂的。甲玛角岩中电气石 Fe/(Fe+Mg) 和 Al 含量变化范围巨大, 表明角岩 Al、Fe、Mg 等对电气石成分影响较大。

6.2 对岩浆热液流体演化的指示

甲玛角岩中的电气石环带十分发育, 成分变化极为复杂, 核部既有镁电气石, 又有黑电气石, 且从核部到边部表现为: (1) Al_2O_3 含量先升高后减低, Fe/(Fe+Mg)、Na/(Na+Ca) 和 TiO_2 先降低后升高; (2) Al_2O_3 和 TiO_2 旋律性变化, Fe/(Fe+Mg) 先升高后减低, Na/(Na+Ca) 先降低后升高; (3) TiO_2 含量先升高后减低, Fe/(Fe+Mg)、Na/(Na+Ca) 和 Al_2O_3 先降低后升高(图 7)。岩浆黑云母是甲玛矿床中酸性斑岩中最主要的富镁铁质矿物, 具有富镁的特征,

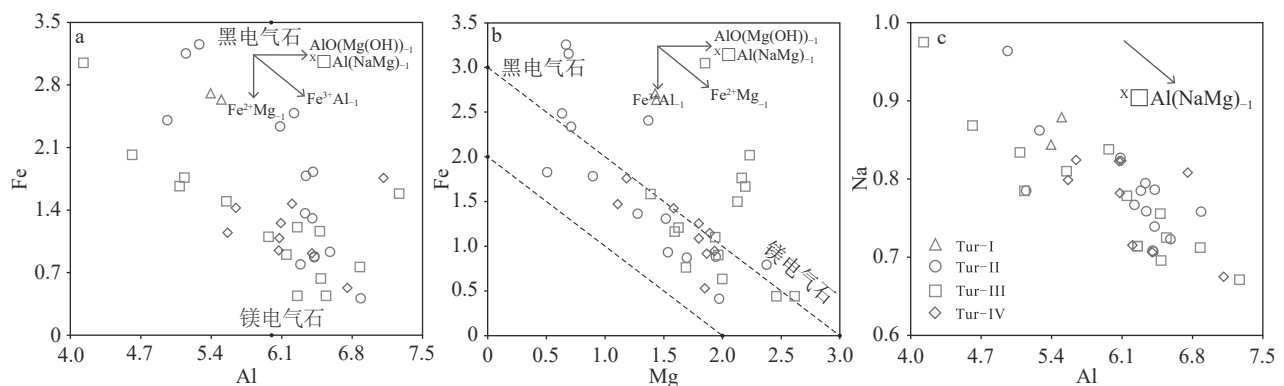


图 6 甲玛不同产状电气石中阳离子占位及元素置换趋势图解

a—Al-Fe 图解; b—Y 位置 Mg-Fe 置换图解; c—Al-Na 图解

Fig.6 Binary plot cation occupancies and exchange vectors in different types of tourmaline in Jiama deposit

a—Plot of Fe vs. Al; b—Plot of Fe vs. Mg in Y-site; c—Plot of Na vs. Al

并且热液黑云母也继承了岩浆黑云母的特征,也具有富镁的特征(唐攀等,2016)。由于大量的黑云母沉淀,造成后期的热液流体具有较高的 Fe/Mg 值,因此推测单纯的从岩浆热液流体结晶的电气石应该具有较高的 Fe/(Mg+Fe) 比值,这与多数电气石有高 Fe 的核部相吻合。

甲玛角岩中电气石环带复杂,且往往存在成分突变的情况;此外,同一条脉体也发育两种成分截然不同的电气石(图8),表明电气石是由两种不同流体混合而成的。Yang et al. (2012)研究表明,在高流体通量环境中,围岩中的硅酸盐矿物为富 B 流体结晶大量电气石提供必要的 Mg-Ca-Al 成分。甲玛角岩的成分较为复杂,原生的斑点状角岩具有

富 Al、Fe 的特征,而遭受黑云母化蚀变的角岩则具有富 Al、Mg 的特征(王崴平和唐菊兴,2011;唐攀等,2016)。通过水岩反应,角岩可能提供两种不同成分的地层流体,一种富 Al、Fe、Ca(原生斑点状角岩),另一种则富 Al、Mg、Ca(黑云母化角岩)。甲玛角岩中电气石环带 Al 和 Ti 呈现相反的变化趋势,可能指示 Ti 主要来自岩浆热液流体,而 Al 则可能更多的来自围岩地层。因此,推测甲玛角岩中复杂的电气石环带类型以及宽泛的 Fe/(Fe+Mg) 等成分,可能是岩浆热液流体和地层流体不同程度的混合造成的,且岩浆热液流体与还原性的角岩地层发生的水岩反应可能在甲玛成矿过程中起了重要作用。

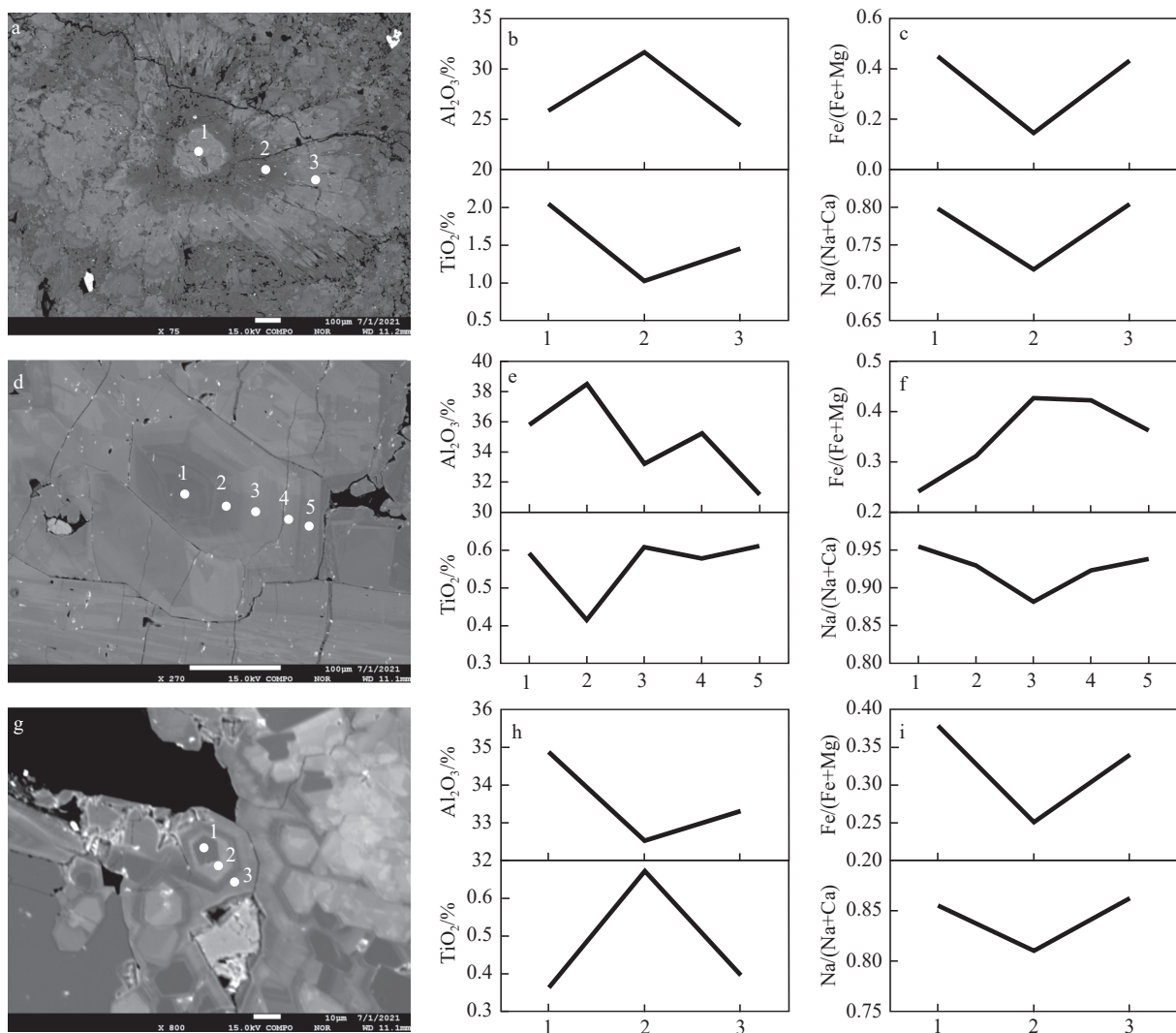


图7 甲玛电气石环带成分趋势图及对应的背散射电子照片
Fig.7 Compositional profiles and the backscattered electronic images of tourmaline zones in Jima deposit

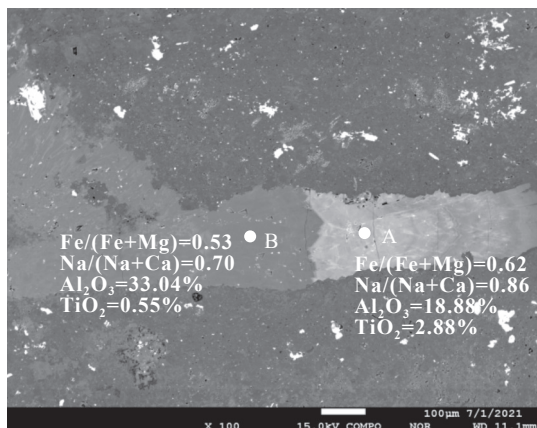


图 8 甲玛电气石脉背散射电子照片
Fig.8 Backscattered electronic image of tourmaline vein

7 结 论

(1) 甲玛矿区角岩中的电气石产状可分为 4 类: Tur-I 热液角砾岩胶结物中电气石, Tur-II 石英+电气石±黄铁矿脉, Tur-III 电气石±黄铁矿±黄铜矿脉, Tur-IV 团斑状电气石±黄铁矿。

(2) 甲玛矿区角岩中不同产状电气石均具有较为宽泛的 Al_2O_3 、 $\text{Fe}/(\text{Fe}+\text{Mg})$ 和 $\text{Na}/(\text{Na}+\text{Ca})$ 比值, 属于碱基亚类镁电气石和黑电气石, 替代机制为 $\text{X}\square\text{Al}(\text{NaMg})_{-1}$ 、 $\text{Fe}^{2+}\text{Mg}_{-1}$ 和 $\text{Fe}^{3+}\text{Al}_{-1}$ 。

(3) 甲玛矿区角岩中不同产状电气石发育复杂的环带类型, 且成分变化极大, 表明其是岩浆热液流体和地层流体不同程度的混合造成的, 且岩浆热液流体与还原性的角岩地层发生的水岩反应可能在甲玛成矿过程中起了重要作用。

References

Allegre J, Courtillot V, Tapponnier P, Hirn A, Mattauer M, Coulon C, Jaeger J J, Achache J, Scharer U, Marcoux J, Burg J P, Girardeau J, Armijo R, Garipey C, Gopel C, Li T, Xiao X C, Chang C F. 1984. Structure and evolution of the Himalaya-Tibet orogenic belt[J]. *Nature*, 307: 17-22.

Baksheev I A, Prokofev V Y, Zaraisky G P, Chitalin A F, Yapaskurt V O, Nikolaev Y N, Tikhomirov P L, Nagornaya E V, Rogacheva L I, Gorelikova N V, Kononov O V. 2012. Tourmaline as a prospecting guide for the porphyry-style deposits[J]. *European Journal of Mineralogy*, 24(6): 957-979.

Chung S L, Chu M F, Zhang Y Q, Xie Y W, Lo C H, Lee T Y, Lan C Y, Li X H, Zhang Q, Wang Y Z. 2005. Tibetan tectonic evolution inferred from spatial and temporal variations in post-collisional

magmatism[J]. *Earth-Science Reviews*, 68: 173-196.

Codeço M S, Weis P, Trumbull R B, Pinto F, Lecumberri-Sanchez P, Wilke F D H. 2017. Chemical and boron isotopic composition of hydrothermal tourmaline from the Panasqueira W-Sn-Cu deposit, Portugal[J]. *Chemical Geology*, 468: 1-16.

Dutrow B L, Henry D J. 2011. Tourmaline: A geologic DVD[J]. *Elements*, 7: 301-306.

Feng Yonggang, Liang Ting, Wang Mengxi, Zhang Ze, Hao Yuanyuan, Cen Jubiao, Dong Ziyuan. 2022. Geochemistry of tourmaline from granitic pegmatites in East Qinling and its implications for mineralization[J]. *Acta Petrologica Sinica*, 38(2): 428-444 (in Chinese with English abstract).

Griffin W L, Slack J F, Ramsden A R, Qin T T, Ryan C G. 1996. Trace elements in tourmalines from massive sulfides deposits and tourmalinites: Geochemical controls and exploration applications [J]. *Economic Geology*, 91(4): 657-675.

Guo Jia, Yan Haibo, Ling Mingxing, Zhang Rongqing. 2020. Chemical composition of tourmaline in the biotite granite, the Dachang district: Insights into magmatic-hydrothermal evolution[J]. *Acta Petrologica Sinica*, 36(1): 171-183 (in Chinese with English abstract).

Guo Wenbo, Zheng Wenbao, Tang Juxing, Ying Lijuan, Wang Yiyun, Lin Bin. 2014. Geochemical constraints on the source of metallogenic fluids and materials in the Jiama polymetallic Cu deposit, Tibet[J]. *Geology in China*, 41(2): 510-528 (in Chinese with English abstract).

Gupta S, Jayananda M, Fareeduddin. 2014. Tourmaline from the Archean G. R. Halli gold deposit, Chitradurga greenstone belt, Dharwar craton (India): Implications for the gold metallogeny[J]. *Geoscience Frontiers*, 5(6): 877-892.

Han J S, Hollings P, Jourdan F, Zeng Y C, Chen H Y. 2020. Inherited Eocene magmatic tourmaline captured by the Miocene Himalayan leucogranites[J]. *American Mineralogist*, 105: 1436-1440.

Harlaux M, Kouzmanov K, Gialli S, Laurent O, Rielli O, Dini A, Chauvet A, Menzies A, Kalinaj M, Fontbot'e L. 2020. Tourmaline as a tracer of late-magmatic to hydrothermal fluid evolution: The world-class San Rafael tin (-copper) deposit, Peru[J]. *Economic Geology*, 115: 1665-1697.

Henry D J, Guidotti C V. 1985. Tourmaline as a petrogenetic indicator mineral: an example from the staurolite-grade metapelites of NW Maine[J]. *American Mineralogist*, 70: 1-15.

Henry D J, Dutrow B L. 1996. Metamorphic tourmaline and its petrologic applications[J]. *Reviews in Mineralogy and Geochemistry*, 33: 503-558.

Henry D J, Novák M, Hawthorne F C, Ertl A, Dutrow B L, Uher P, Pezzotta F. 2011. Nomenclature of the tourmaline-supergroup minerals[J]. *American Mineralogist*, 96: 895-913.

Hinsberg V J V, Henry D J, Marschall H R. 2011. Tourmaline: An ideal indicator of its host environment[J]. *The Canadian Mineralogist*, 49: 1-16.

Hou Z Q, Ma H W, Zaw K, Zhang Y Q. 2003. The Himalayan Yulong

- porphyry copper belt: Product of large-scale strike-slip faulting in Eastern Tibet[J]. *Economic Geology*, 98(1): 125–145.
- Hou Zengqian, Yang Zhusen, Xu Wenyi, Mo Xuanxue, Ding Lin, Gao Yongfeng, Dong Fangliu, Li Guangming, Qu Xiaoming, Zhao Zhidan, Jiang Sihong, Meng Xiangjin, Li Zhenqing, Qin Kezhang, Yang Zhiming. 2006. Metallogenesis in Tibetan collisional orogenic belt: I. Mineralization in main-collisional transformation setting[J]. *Mineral Deposits*, 25 (4): 337–358 (in Chinese with English abstract).
- Jia R X, Fang W X, Hu R Z. 2010. Mineral geochemical compositions of tourmalines and their significance in the Gejiu Tin polymetallic deposits, Yunnan, China[J]. *Acta Geologica Sinica*, 84(1): 155–166.
- Lang X H, Tang J X, Li Z J, Huang Y, Ding F, Yang H H, Zhou Y. 2014. U–Pb and Re–Os geochronological evidence for the Jurassic porphyry metallogenic event of the Xiongcu district in the Gangdese porphyry copper belt, southern Tibet, PRC[J]. *Journal of Asian Earth Sciences*, 79: 608–622.
- Launay G, Sizareta S, Guillou–Frotier L, Gloaguen E, Pinto F. 2018. Deciphering fluid flow at the magmatic–hydrothermal transition: A case study from the world-class Panasqueira W–Sn–(Cu) ore deposit (Portugal)[J]. *Earth and Planetary Science Letters*, 499: 1–12.
- Li Zhenzhen, Qin Kezang, Pei Bin, Zhao Junxing, Shi Ruize, Zhao Zelong, Han Ri. 2020. Mineralogical features of tourmaline in Baiyinchagan Sn–Ag–Pb–Zn deposit, southern Great Xing'an Range, and its implications for magmatic–hydrothermal evolution[J]. *Acta Petrologica Sinica*, 36(12): 3797–3812 (in Chinese with English abstract).
- Lin Bin, Tang Juxing, Tang Pan, Zheng Wenbao, Greg Hall, Chen Guoliang, Zhang Zhongkun. 2019. Polycentric complex mineralization model of porphyry system: A case study of Jiama superlarge deposit in Tibet[J]. *Mineral Deposits*, 38(6): 1204–1222 (in Chinese with English abstract).
- Lin Bin, Tang Juxing, Tang Pan, Zhou Aorigele, Sun Miao, Qi Jing, Chen Guoliang, Zhang Zhongkun, Zhang Zebin, Wu Chunneng, Tian Zhichao, Dai Jingjing, Yang Zhengkun, Yao Xiaofeng. 2021. Preliminary study of first 3000 m scientific drilling in Jiama porphyry metallogenic system, Tibet[J]. *Mineral Deposits*, 40(6): 1119–1134 (in Chinese with English abstract).
- London D, Manning D A C. 1995. Chemical variation and significance of tourmaline from Southwest England[J]. *Economic Geology*, 90(3): 495–519.
- Mo X X, Hou Z Q, Niu Y L, Dong G C, Qu X M, Zhao Z D, Yang Z M. 2007. Mantle contributions to crustal thickening during continental collision: Evidence from Cenozoic igneous rocks in southern Tibet[J]. *Lithos*, 96: 225–242.
- Mo X X, Niu Y L, Dong G C, Zhao Z D, Hou Z Q, Zhou S, Ke S. 2008. Contribution of syncollision felsic magmatism to continental crust growth: A case study of the Paleogene Linzizong volcanic succession in southern Tibet[J]. *Chemical Geology*, 250: 49–67.
- Novák M, Koda R, Filip J, Macek I, Vaculovi T. 2011. Compositional trends in tourmaline from intragranitic NYF pegmatites of the terbic pluton, Czech Republic: An electron microprobe, Mossbauer and LA–ICP–MS study[J]. *The Canadian Mineralogist*, 49(1): 359–380.
- Qiu K F, Yu H C, Hetherington C, Huang Y Q, Yang T, Deng J. 2021. Tourmaline composition and boron isotope signature as a tracer of magmatic–hydrothermal processes[J]. *American Mineralogist*, 106: 1033–1044.
- Slack J F, Trumbull R B. 2011. Tourmaline as a recorder of ore-forming processes[J]. *Elements*, 7: 321–326.
- Tang Juxing, Deng Shilin, Zheng Wenbao, Ying Lijuan, Wang Xiongwu, Zhong Kanghui, Qin Zhipeng, Ding Feng, Li Fengji, Tang Xiaoqian, Zhong Yufeng, Peng Huijuan. 2011. An exploration model for Jiama copper polymetallic deposit in Maizhokunggar County, Tibet[J]. *Mineral Deposits*, 30(2): 179–196 (in Chinese with English abstract).
- Tang Juxing, Duo Ji, Liu Hongfei, Lang Xinghai, Zhang Jinshu, Zheng Wenbao, Ying Lijuan. 2012. Mineralogical series of ore deposits in the east part of the Gangdise metallogenic belt[J]. *Acta Geoscientia Sinica*, 33(4): 393–410 (in Chinese with English abstract).
- Tang Juxing, Wang Denghong, Wang Xiongwu, Zhong Kanghui, Ying Lijuan, Zheng Wenbao, Li Fengjie, Guo Na, Qin Zhipeng, Yao Xiaofeng, Li Lei, Wang You, Tang Xiaoqian. 2010. Geological features and metallogenic model of the Jiama copper–polymetallic deposit in Tibet[J]. *Acta Geoscientia Sinica*, 31(4): 495–506 (in Chinese with English abstract).
- Tang Juxing, Wang Qin, Yang Huanhuan, Gao Xin, Zhang Zebin, Zou Bin. 2017. Mineralization, exploration and resource potential of porphyry–skarn–epithermal copper polymetallic deposits in Tibet[J]. *Acta Geoscientia Sinica*, 38(5): 571–613 (in Chinese with English abstract).
- Tang P, Tang J X, Lin B, Wang L Q, Zheng W B, Leng Q F, Gao X, Zhang Z B, Tang X Q. 2019. Mineral chemistry of magmatic and hydrothermal biotites from the Bangpu porphyry Mo (Cu) deposit, Tibet[J]. *Ore Geology Reviews*, 115: 103122.
- Tang P, Tang J X, Wang Y, Lin B, Zheng W B, Leng Q F, Zhang Z B, Yang Y, Wu C N, Qi J, Li Y X. 2020. Zircon U–Pb geochronology, geochemistry, S–Pb–Hf isotopic compositions, and mineral chemistry of the Xin'gaguo skarn Pb–Zn deposit, Tibet, China[J]. *Geological Journal*, 55(6): 4790–4809.
- Tang P, Tang J X, Wang Y, Lin B, Leng Q F, Zhang Q Z, He L, Zhang Z B, Sun M, Wu C N, Qi J, Li Y X, Dai S J. 2021. Genesis of the Lakang'e porphyry Mo (Cu) deposit, Tibet: Constraints from geochemistry, geochronology, Sr–Nd–Pb–Hf isotopes, zircon and apatite[J]. *Lithos*, 380–381: 1–38.
- Tang Pan, Tang Juxing, Zheng Wenbao, Leng Qiufeng, Lin Bin, Tang Xiaoqian, Wang Hao, Gao Xin, Zhang Zebin, Zhou Hongbing. 2017. Is Tongshan orebody in the Jiama copper–polymetallic Deposit Manto-type ore?[J]. *Acta Geoscientia Sinica*, 38(5):

- 829–838 (in Chinese with English abstract).
- Tang Pan, Chen Yuchuan, Tang Juxing, Zheng Wenbao, Leng Qiufeng. 2016. Characteristics and geological significance of biotites in Jiama porphyry deposit system, Tibet[J]. *Mineral Deposits*, 35(4): 846–866 (in Chinese with English abstract).
- van Hinsberg V J, Henry D J, Marschall H R. 2011. Tourmaline: An ideal indicator of its host environment[J]. *The Canadian Mineralogist*, 49: 1–16.
- Wang Denghong, Tang Juxing, Ying Lijuan, Lin Bin, Ding Shuai. 2011. Hornfels feature in the Jiama ore deposit, Tibet and its significance on deep prospecting[J]. *Acta Petrologica Sinica*, 27(7): 2103–2108 (in Chinese with English abstract).
- Wang L Q, Tang J X, Yang Y, Li Z, Lin B. 2018. Zircon U–Pb geochronology, geochemistry, and S–Pb isotopic compositions of the Lietinggang iron polymetallic deposit, Tibet, China[J]. *Ore Geology Review*, 98: 62–79.
- Wang Weiping, Tang Juxing. 2011. Rock types and genetic significance of hornfels and location prediction of concealed porphyry bodies in Jiama copper polymetallic deposit, Tibet[J]. *Mineral Deposits*, 30(6): 1017–1038 (in Chinese with English abstract).
- Wang Yiyun, Zheng Wenbao, Chen Yuchuan, Tang Juxing, Leng Qiufeng, Tang Pan, Ding Shuai, Zhou Yun. 2017. Discussion on the mechanism of separation of copper and molybdenum in Jiama porphyry deposit system, Tibet[J]. *Acta Petrologica Sinica*, 33(2): 495–514 (in Chinese with English abstract).
- Xie F W, Tang J X, Chen Y C, Lang X H. 2018. Apatite and zircon geochemistry of Jurassic porphyries in the Xiongcu district, southern Gangdese porphyry copper belt: Implications for petrogenesis and mineralization[J]. *Ore Geology Reviews*, 96: 98–114.
- Xue Jianling, Xu Hong, Gao Yiming, Huang Jingyi. 2006. Mineralogical characteristics of tourmaline in the Houxianyu boron deposit in Liaoning and their significance for rock and ore formation[J]. *Geology in China*, 33(6): 1386–1392 (in Chinese with English abstract).
- Yang S Y, Jiang S Y, Zhao K D, Jiang Y H, Ling H F, Luo L. 2012. Geochronology, geochemistry and tectonic significance of two Early Cretaceous A–type granites in the Gan–Hang Belt, Southeast China[J]. *Lithos*, 150: 155–170.
- Yang Z M, Cooke D R. 2019. Porphyry copper deposits in China[J]. *Society of Economic Geologists Special Publication*, 22: 133–187.
- Yang Z M, Hou Z Q, White N C, Chang Z S, Li Z Q, Song Y. 2009. Geology of the post–collisional porphyry copper–molybdenum deposit at Qulong, Tibet[J]. *Ore Geology Review*, 36: 133–159.
- Yao Xiaofeng, Ye Tianzhu, Tang Juxing, Zheng Wenbao, Ding Shuai, Li Yongsheng, Zheng Shimin. 2014. The effect of Si–Ca interface on skarn formation and polymetallic mineralization in the Jiama deposit, Tibet[J]. *Geology in China*, 41(5): 1577–1593 (in Chinese with English abstract).
- Yin A, Harrison T M. 2000. Geologic evolution of the Himalayan–Tibetan orogen[J]. *Annual Review of Earth and Planetary Sciences*, 28: 211–280.
- Ying Lijuan, Tang Juxing, Wang Denghong, Zheng Wenbao, Qin Zhipeng, Zhang Li. 2011. Zircon shrimp U–Pb dating of porphyry vein from the Jiama copper polymetallic deposit in Tibet and its significance[J]. *Acta Petrologica Sinica*, 27(7): 2095–2102 (in Chinese with English abstract).
- Ying Lijuan, Wang Denghong, Tang Juxing, Chang Zhesheng, Qu Wenjun, Zheng Wenbao, Wang Huan. 2010. Re–Os dating of molybdenite from the Jiama copper polymetallic deposit in Tibet and its metallogenic significance[J]. *Acta Geologica Sinica*, 84(8): 1165–1174 (in Chinese with English abstract).
- Yu J M, Jiang S Y. 2003. Chemical composition of tourmaline from the Yunlong tin deposit, Yunnan, China: Implications for ore genesis and mineral exploration[J]. *Mineralogy and Petrology*, 77(1): 67–84.
- Yu M, Feng C Y, Mao J W, Zhao Y M, Li D X. 2017. Multistage skarn–related tourmaline from Galinge deposit, Qiman Tagh, western China: A fluid evolution perspective[J]. *The Canadian Mineralogist*, 55: 3–19.
- Yu Miao, Feng Chengyou, Liu Hongchuan, Li Dingwu, Zhao Yiming, Li Daxin, Liu Jiannan, Wang Hui. 2016. Mineralogy, element geochemistry and genesis of tourmaline from Galinge skarn deposit, Qinghai Province[J]. *Mineral Deposits*, 35(1): 69–84 (in Chinese with English abstract).
- Zhang S T, Lu J J, Zhang R Q, Liang X L, Ma D S, Li R C, Wu J W. 2021. Tourmaline as an indicator for late–magmatic to hydrothermal fluid evolution of the Neoproterozoic Baotan tin deposit, South China[J]. *Ore Geology Review*, 139: 104504.
- Zhang Z M, Dong X, Santosh M, Zhao G C. 2014. Metamorphism and tectonic evolution of the Lhasa terrane, Central Tibet[J]. *Gondwana Research*, 25: 170–189.
- Zhang Zebin, Tang Juxing, Tang Pan, Chen Guoliang, Zhang Zhongkun, Gao Xin, Yang Yang. 2019. The origin of the mafic microgranular enclaves from Jiama porphyry Cu polymetallic deposit, Tibet: Implications for magma mixing/mingling and mineralization[J]. *Acta Petrologica Sinica*, 35(3): 934–952 (in Chinese with English abstract).
- Zhang Zhongkun, Lin Bin, Chen Guoliang, Zou Bing, Yang Zhengkun, Tang Pan, Gao Xin, Qi Jing, Li Faqiao, Gao Futai, Jiao Haijun, Sun Jianjun, Li Yajun, Su Wei. 2021. The diagenesis–mineralization–structure coupling relationship of South–Pit skarn thick ore body in the Jiama super large–sized deposit, Tibet[J]. *Geology in China*, 48(6): 1804–1817 (in Chinese with English abstract).
- Zhao X Y, Yang Z S, Zheng Y C, Liu Y C, Tian S H, Fu Q. 2015. Geology and genesis of the post–collisional porphyry–skarn deposit at Bangpu, Tibet[J]. *Ore Geology Reviews*, 70: 486–509.
- Zheng W B, Tang J X, Zhong K H, Ying L J, Leng Q F, Ding S, Lin B. 2016. Geology of the Jiama porphyry copper–polymetallic system,

- Lhasa Region, China[J]. *Ore Geology Reviews*, 74: 151–169.
- Zhong Kanghui, Li Lei, Zhou Huiwen, Bai Jingguo, Li Wei, Zhong Wanting, Zhang Yongqiang, Lin Jiqing, Zheng Fanshi, Huang Xiaoyu, Lu Biao, Lei Bo. 2012. Features of Jiama (Gyama)–Kajunguo thrust–gliding nappe tectonic[J]. *Acta Geoscientica Sinica*, 33(4): 411–423 (in Chinese with English abstract).
- Zhu D C, Zhao Z D, Niu Y, Dilek Y, Hou Z Q, Mo X X. 2013. The origin and pre-Cenozoic evolution of the Tibetan Plateau[J]. *Gondwana Research*, 23: 1429–1454.
- ### 附中文参考文献
- 凤永刚, 梁婷, 王梦玺, 张泽, 郝媛媛, 岑炬标, 董紫. 2022. 东秦岭花岗岩伟晶岩中电气石地球化学特征及成矿指示意义[J]. *岩石学报*, 38(2): 428–444.
- 郭佳, 严海波, 凌明星, 章荣清. 2020. 广西大厂地区黑云母花岗岩中电气石的化学组成及其对岩浆热液演化的指示[J]. *岩石学报*, 36(1): 171–183.
- 郭文铂, 郑文宝, 唐菊兴, 应立娟, 王艺云, 林彬. 2014. 西藏甲玛铜多金属矿床流体、成矿物质来源的地球化学约束[J]. *中国地质*, 41(2): 510–528.
- 侯增谦, 杨竹森, 徐文艺, 莫宣学, 丁林, 高永丰, 董方洵, 李光明, 曲晓明, 李光明, 赵志丹, 江思宏, 孟祥金, 李振清, 秦克章, 杨志明. 2006. 青藏高原碰撞造山带: I. 主碰撞造山成矿作用[J]. *矿床地质*, 25(4): 337–358.
- 李真真, 秦克章, 裴斌, 赵俊兴, 施睿哲, 赵泽龙, 韩日. 2020. 大兴安岭南段白音查干 Sn–Ag–Zn–Pb 矿床电气石矿物学特征及对岩浆–热液演化过程的启示[J]. *岩石学报*, 36(12): 3797–3812.
- 林彬, 唐菊兴, 唐攀, 郑文宝, Greg Hall, 陈国良, 张忠坤. 2019. 斑岩成矿系统多中心复合成矿作用模型——以西藏甲玛超大型矿床为例[J]. *矿床地质*, 38(6): 1204–1222.
- 林彬, 唐菊兴, 唐攀, 周敖日格勒, 孙渺, 祁婧, 陈国良, 张忠坤, 张泽斌, 吴纯能, 田志超, 代晶晶, 杨征坤, 姚晓峰. 2021. 青藏高原甲玛斑岩成矿系统首例 3000 m 科学深钻的初步认识[J]. *矿床地质*, 40(6): 1119–1134.
- 唐菊兴, 邓世林, 郑文宝, 应立娟, 汪雄武, 钟康惠, 秦志鹏, 丁枫, 黎枫佶, 唐晓倩, 钟裕峰, 彭慧娟. 2011. 西藏墨竹工卡县甲玛铜多金属矿床勘查模型[J]. *矿床地质*, 30(2): 179–196.
- 唐菊兴, 多吉, 刘鸿飞, 郎兴海, 张金树, 郑文宝, 应立娟. 2012. 冈底斯成矿带东段矿床成矿系列及找矿突破的关键问题研究[J]. *地球学报*, 33(4): 393–410.
- 唐菊兴, 王登红, 汪雄武, 钟康惠, 应立娟, 郑文宝, 黎枫佶, 郭娜, 秦志鹏, 姚晓峰, 李磊, 王友, 唐晓倩. 2010. 西藏甲玛铜多金属矿床地质特征及其矿床模型[J]. *地球学报*, 31(4): 495–506.
- 唐菊兴, 王勤, 杨欢欢, 高昕, 张泽斌, 邹兵. 2017. 西藏斑岩–矽卡岩–浅成低温热液铜多金属矿成矿作用、勘查方向与资源潜力[J]. *地球学报*, 38(5): 571–613.
- 唐攀, 陈毓川, 唐菊兴, 郑文宝, 冷秋锋, 林彬. 2016. 西藏甲玛斑岩矿床系统黑云母特征及其地质意义[J]. *矿床地质*, 35(4): 846–866.
- 唐攀, 唐菊兴, 郑文宝, 冷秋锋, 林彬, 唐晓倩, 王豪, 高昕, 张泽斌, 周洪兵. 2017. 西藏甲玛铜多金属矿床铜山矿体为 manto 型矿体? [J]. *地球学报*, 38(5): 829–838.
- 王登红, 唐菊兴, 应立娟, 林彬, 丁帅. 2011. 西藏甲玛矿区角闪岩特征及其对深部找矿的意义[J]. *岩石学报*, 27(7): 2103–2108.
- 王崑平, 唐菊兴. 2011. 西藏甲玛铜多金属矿床角闪岩类型、成因意义及隐伏斑岩岩体定位预测[J]. *矿床地质*, 30(6): 1017–1038.
- 王艺云, 郑文宝, 陈毓川, 唐菊兴, 冷秋锋, 唐攀, 丁帅, 周云. 2017. 西藏甲玛斑岩成矿系统铜铅元素分离机制探讨[J]. *岩石学报*, 33(2): 495–514.
- 薛建玲, 许虹, 高一鸣, 黄静宜. 2006. 辽宁后仙峪矿床中电气石的矿物学特征及其成岩成矿意义[J]. *中国地质*, 33(6): 1386–1392.
- 姚晓峰, 叶天竺, 唐菊兴, 郑文宝, 丁帅, 李永胜, 甄世民. 2014. 西藏甲玛矿床硅钙界面对矽卡岩成岩及多金属成矿的影响[J]. *中国地质*, 41(5): 1577–1593.
- 应立娟, 唐菊兴, 王登红, 郑文宝, 秦志鹏, 张丽. 2011. 西藏甲玛超大型铜矿区斑岩脉成岩时代及其与成矿的关系[J]. *岩石学报*, 27(7): 2095–2102.
- 应立娟, 王登红, 唐菊兴, 畅哲生, 屈文俊, 郑文宝, 王煥. 2010. 西藏甲玛铜多金属矿辉钼矿 Re–Os 定年及其成矿意义[J]. *地质学报*, 84(8): 1165–1174.
- 于森, 丰成友, 刘洪川, 李定武, 赵一鸣, 李大新, 刘建楠, 王辉. 2016. 青海杂林格铁矿床电气石矿物学、元素地球化学及成因研究[J]. *矿床地质*, 35(1): 69–84.
- 张泽斌, 唐菊兴, 唐攀, 陈国良, 张忠坤, 高昕, 杨阳. 2019. 西藏甲玛铜多金属矿床暗色包体岩石成因: 对岩浆混合和成矿的启示[J]. *岩石学报*, 35(3): 934–952.
- 张忠坤, 林彬, 陈国良, 邹兵, 杨征坤, 唐攀, 高昕, 祁婧, 李发桥, 高福太, 焦海军, 孙建军, 李亚军, 苏伟. 2021. 西藏甲玛超大型矿床南坑厚大矽卡岩矿体的成岩–成矿–构造耦合关系[J]. *中国地质*, 48(6): 1804–1817.
- 钟康惠, 李磊, 周慧文, 白景国, 李伟, 钟婉婷, 张勇强, 蔺吉庆, 郑凡石, 黄小雨, 陆彪, 雷波. 2012. 西藏甲玛–卡军果推–滑覆构造系特征[J]. *地球学报*, 33: 411–423.